# Metastable state of the photomagnetic Prussian blue analog $K_{0.3}Co[Fe(CN)_6]_{0.77}\cdot 3.6H_2O$ investigated by various techniques

Christian Chong,[*] Miho Itoi,[†] Kamel Boukheddaden,[‡] Epiphane Codjovi, Aurelian Rotaru,[§] and François Varret[‖]
*Groupe d'Etudes de la Matière Condensée, UMR 8635, CNRS-Université de Versailles Saint-Quentin-en-Yvelines, 45 Avenue des Etats Unis, FR-78035 Versailles, France*

Franz A. Frye and Daniel R. Talham
*Department of Chemistry, University of Florida, Gainesville, Florida 32611-7200, USA*

Isabelle Maurin
*Laboratoire de Physique de la Matière Condensée, UMR 7643, CNRS-Ecole Polytechnique, Route de Saclay, FR-91120 Palaiseau, France*

Dmitry Chernyshov
*Swiss-Norwegian Beam-Lines, European Synchrotron Radiation Facility, BP 220, FR-38048 Grenoble Cedex, France*

Miguel Castro
*Instituto de Ciencia de Materiales de Aragón, CSIC-Universidad de Zaragoza, Pedro Cerbuna 12, ES-50009 Zaragoza, Spain*
(Received 13 July 2009; revised manuscript received 9 May 2011; published 4 October 2011)

The thermodynamic properties of the photomagnetic Prussian blue analog $K_{0.3}Co[Fe(CN)_6]_{0.77}\cdot 3.6H_2O$, which exhibits a charge-transfer-induced spin transition (CTIST), are reported. According to the thermal history of the sample, different low-temperature states are obtained: a quenched high-spin state (Q), a low-spin state (LT) achieved through the decay of the Q state, and an intermediate state (IM) combining low-spin (LS) and high-spin (HS) local states. The IM state is obtained by slow cooling and displays a slight kinetic dependence. The long lifetime of the IM state, which persists up to the vicinity of the CTIST temperature, is unusual and differs from all metastable states reported so far for photomagnetic Prussian blue analogs. The properties of the different states and of their photoexcited counterparts are investigated by magnetic and photomagnetic measurements, calorimetry, diffuse reflectance, and x-ray diffraction. A key feature of the IM state revealed by x-ray diffraction is the onset of phase separation between a LT-type fraction and a mixed HS-LS fraction (approximately 50 : 50). X-ray patterns of the IM state obtained during successive cooling and heating stages document irreversible transformations. The formation and properties of the IM state suggest a self-organization process between low- and high-spin sites in response to internal structural stresses, and this effect is hindered by irradiation with visible light. The relaxation kinetics of the Q and photoexcited states are analyzed by using a two-variable model, which accounts for the onset of correlations due to short-range elastic interactions. A quantitative comparison to the analogous sodium compound $Na_{0.32}Co[Fe(CN)_6]_{0.74}\cdot 3.4H_2O$ confirms the nonstandard behavior of the title potassium compound and supports the structural origin of the self-organization processes.

DOI: 10.1103/PhysRevB.84.144102 PACS number(s): 75.50.Xx, 75.30.Wx, 64.60.My, 64.70.K−

## I. INTRODUCTION

Prussian blue analogs (PBAs) have attracted a great deal of interest since high-$T_C$ examples were discovered in 1995 by the Verdaguer group[1] and the subsequent 1996 report of photoinduced magnetization in examples by the Hashimoto group.[2] The latter property opened the possibility of integrating PBAs into magneto-optical devices and provided an important new class of switchable molecular materials.[3–7] While the electronic mechanism involved in the thermally and photoinduced transitions has been recently elucidated, the associated structural aspects remain relatively unstudied. Short-range structural modifications in $A_xCo[Fe(CN)_6]_y\cdot zH_2O$ (A: alkali metal) PBAs were observed in 1998 by extended x-ray absorption fine structure (EXAFS),[8,9] but complete analysis of the long-range aspects remains to be investigated. These structural modifications are obviously involved in the multistability previously reported for some PBAs,[10] and might play a key role in the control of the photoinduced magnetic phases.

The electronic switching in the Co-Fe–based PBAs is described as a charge-transfer-induced spin transition (CTIST),[2] which occurs between active Co-Fe pairs

$$\mathrm{Co^{III}(S=0)\text{-}Fe^{II}(S=0)} \leftrightarrow \quad \text{(low temperature)}$$
$$\mathrm{Co^{II}(S=3/2)\text{-}Fe^{III}(S=1/2)}, \quad \text{(high temperature)}$$

where the $Fe^{2+}$ to $Co^{3+}$ electron transfer is associated with a low-spin (LS) to high-spin (HS) transition of the cobalt ion. The electron transfer and spin-state change can not be trivially disentangled, but can be considered as successive steps for the photoinduced transition.[11,12] The condition for a pair to be active has been analyzed in terms of the redox potential difference of the metal atoms and depends on the density of $[Fe(CN)_6]^{3-}$ vacancies in the system.[13]

Upon rapid cooling, CTIST PBAs can be quenched and trapped at low temperature in the high-temperature state. Spin

 

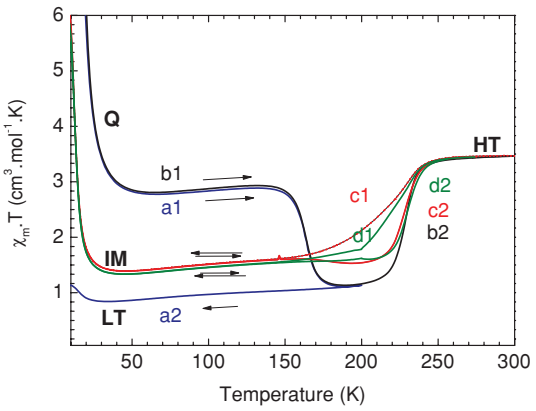


FIG. 1. (Color online) Temperature dependences of the $\chi_m \cdot T$ product, obtained with the bulk sample under 0.1 T applied field. Blue (a) and black (b) curves start from the thermally quenched state. The red (c) and green (d) curves start from room temperature, at a controlled temperature scan rate: 1 and 0.1 K/min, respectively. The different low-temperature states are labeled Q (after thermal quenching), LT (after relaxation of the Q state), and IM (intermediate state).

crossover (SC) and PBA compounds have provided examples of efficient quenching, which can be obtained when the gap between the thermal transition temperature and the thermal return temperature, often called $T_{LIESST}$ (Ref. 14) for the SC compounds, is narrow enough to prevent sizable relaxation of the metastable HS state during the cooling process. The ability of such systems to be thermally quenched in the high temperature (HT) state makes it possible to investigate the differences between the thermally quenched and photoinduced metastable states, previously called multimetastability.[15] It is also important to recall that the presence of magnetic interactions in PBAs leads to large photomagnetic effects at low temperature,[16–19] so low-temperature magnetic data can be used, as a first approach, for differentiating the various metastable states of the system.

Efficient quenching was recently observed for $Na_{0.32}Co[Fe(CN)_6]_{0.74} \cdot 3.4H_2O$ using magnetic, Mössbauer,[20] and calorimetric measurements.[21] This paper extends these studies to the potassium analog $K_{0.3}Co[Fe(CN)_6]_{0.77} \cdot 3.6H_2O$, which exhibits an intermediate state (IM) upon slow cooling below the CTIST temperature. This unusual state has magnetic susceptibility values in-between those expected for the low- and high-spin states, with a large hysteresis,[22] the kinetic nature of which is shown in Fig. 1. This paper reports on photomagnetic, diffuse reflectance, calorimetric, and x-ray diffraction investigations. For convenience, the discussion of structural data is restricted to a comparison of the as-synthesized compound and the IM state, leaving a complete investigation of the structural aspects to follow in a separate paper.[23]

## II. EXPERIMENTAL SECTION

### A. Reagents, synthesis, and chemical analysis

Chemical precursors were obtained from Sigma-Aldrich and used as received. Deionized water was obtained from a Barnstead NANOpure system. A reddish brown powder was obtained by dropwise combination of three different nanopure water solutions: $Co(NO_3)_2 \cdot 6H_2O$ (0.005 mol in 50 mL $H_2O$); $K_3Fe(CN)_6$ (0.02 mol in 200 mL $H_2O$); and $KNO_3$ (0.1 mol in 50 mL $H_2O$). The powder was extracted by centrifugation and then dried in vacuum. Infrared (IR) spectra using KBr pellets were recorded on a Thermo Scientific Nicolet 6700 spectrometer in order to characterize the Fe-CN-Co vibrations ($\nu_{CN}$). Bands at 2155 cm$^{-1}$ (strong), 2114 cm$^{-1}$ (medium), and 2092 cm$^{-1}$ (weak), respectively, are assigned to Fe(III)Co(II), Fe(II)Co(III), Fe(II)Co(II) pairs.[18] Energy dispersive x-ray spectroscopy (EDS) was conducted on a JEOL 2010F instrument at the Major Analytical Instrumentation Center at the University of Florida, in order to determine the transition-metal content (Co/Fe) 56.39/43.57. The K/Co content was inferred from electro-neutrality, using the room-temperature valence state $Fe(II)_{0.08}$-$Fe(III)_{0.92}$ from unpublished Mössbauer data. The C, N, H content was determined by combustion analysis at the University of Florida Spectroscopic Services Laboratory. The final formulation was expressed as $K_{0.3}Co[Fe(CN)_6]_{0.77} \cdot 3.6H_2O$. The calculated combustion analysis percentages for $C_{4.6}H_{7.2}N_{4.6}O_{3.6}K_{0.32}Co_{1.0}Fe_{0.77}$ are C, 18.5; H, 2.4; N, 21.5. The measured percentages are C, 18.36; H, 2.06; N, 21.90.

Direct current (dc) magnetization under 0.1 T applied field was measured by a SQUID magnetometer (Quantum Design MPMS-5) equipped with an optical fiber. Irradiation was provided by a 100-W tungsten lamp with 750-nm filter (50-nm bandwidth). Typical intensity was 15 mW/cm$^2$. For the photomagnetic measurements, a thin layer of powder sample was fixed onto a transparent double-stick tape located at the tip of the optical fiber. The complete photomagnetic system was described in a previous work.[24] The mass of the thin sample (~0.64 mg) was obtained by comparison to the room-temperature data of the bulk sample (18.5 mg) used for measurements in the dark, after systematic correction of the diamagnetic contribution of the photomagnetic sample holder.[24] Susceptibilities were corrected for diamagnetic contributions by using literature values.[25]

Calorimetric measurements were performed using a differential scanning calorimeter (DSC) Q1000 from TA Instruments. The low-temperature range was obtained using a liquid-nitrogen cooling system allowing reaching and stabilizing 93 K in the sample holder. The measurements were carried out using around 4 mg of powder sample sealed in aluminum capsules with a mechanical crimp and at a scan rate of 1 K/min. The experiment with the quenched sample was performed after immersing the capsule into liquid nitrogen followed by rapid transfer to the DSC cryostat, opened at 93 K under a flow of helium gas. The calibration procedure was already reported in Ref. 21. The diffuse reflectance device was described in Ref. 26. The irradiation system was the same as that used for the photomagnetic measurements.

The synchrotron x-ray powder diffraction (XPD) measurements were performed at Swiss-Norwegian Beam-Lines (station BM1A) at the European Synchrotron Radiation Factory (France). The powder sample was sealed in a 0.1-mm-diameter Lindemann glass capillary. The diffraction patterns were collected with an imaging plate detector by exposing the sample for 90 seconds to a monochromatic x-ray beam, $\lambda =$ 0.726 89 Å. The as-grown sample was fine enough and gave a homogeneous intensity distribution in the Debye-Sherrer

rings. $LaB_6$ standard powder (NIST) was used to calibrate the sample-to-detector distance, the beam center, and the tilt angle of the image plate detector. For the temperature-dependent measurements, an Oxford Cryostream $N_2$ blower was used for temperature control between 80 and 300 K. For quenching, the sample was directly cooled to 80 K from room temperature. The spontaneous charge-transfer transition and thermal relaxation processes were investigated with 1 K/min scan rate.

## III. RESULTS AND DISCUSSION

### A. Magnetic measurements

The temperature-dependent magnetic response measured in the dark is shown in Fig. 1. The sample was rapidly cooled down to ∼50 K by fast insertion into the precooled sample space of the SQUID magnetometer to achieve the quenched state. It was subsequently warmed (1 K/min) until thermal relaxation was complete (∼200 K) and then cooled again to achieve the LT state, before rewarming to record the spontaneous CTIST, observed here at 230 K [inflection point of the $\chi_M \cdot T(T)$ curve]. The unusual onset of an intermediate low-temperature state (IM), reported by Park *et al.*,[22] was reproduced upon slow cooling and was shown to be sizably dependent on the temperature scan rate. The slow evolution of the system below the CTIST explains why the thermal quenching process is rather efficient in spite of the wide temperature range that separates the CTIST temperature (∼230 K) and the thermal return temperature (∼160 K) (Fig. 1). As it will be shown in the following, the amount of HT state trapped by rapid cooling sensitively depends on the heat capacity of the sample holder. Furthermore, detailed x-ray synchrotron investigations of the system[23] confirmed that the first quenching was virtually complete, but following cycles were not, suggesting some fatigue of the sample generated by the successive thermoswitching and photoswitching experiments. A similar aging effect was observed on the Na compound, presumably arising from the large volume change $\Delta V/V$ ∼9%, which accompanies the spin transition.

Using a thin-layer sample fixed on the tip of the sample holder, we repeated identical sequences to form the low-temperature states: quenched (Q), relaxed quenched (LT), and slowly cooled (IM) states. Photoexcitation was performed at 6 K at 750 nm, 15 mW/cm$^2$, for 3 h, starting either from the LT state or from the IM state to produce the LTPX and IMPX states, respectively (PX indicates a photoexcited state). We first recorded the thermal variation of the resulting magnetic moment in the 6–40 K temperature range to measure the magnetic ordering temperature [actually, the spin-freezing temperature of the cluster-glass state[19] (see Fig. 2)].

The M-H scans were then recorded at low temperature (6 K) to determine the saturation magnetization and coercive field values of the system (see Fig. 3). Finally, the sample was warmed at constant scan rate (1 K/min) to determine the thermal return temperatures of the different metastable states (see Fig. 4).

The main data derived from Figs. 1–4 have been summarized in Table I. The qualitative findings are as follows: (i) Neither the quenching nor the photoexcitation processes are complete. The lower efficiency of the quenching process with respect to the bulk sample (Fig. 1) is explained by the impact of the heat capacity of the sample holder upon the effective cooling rate. On the other hand, the HS content of the IM state in both samples is the same. (ii) The magnetic properties of the Q state sizably depend on the HS content. (iii) The IM state has magnetic properties similar to those of the Q state with 55% HS content. (iv) The Q and LTPX states clearly decay to the same LT state (this result was confirmed by synchrotron XRD, see Ref. 23). (v) The thermal decay occurs more progressively for the photoexcited (PX) states than for the Q state. (vi) The decay of the IMPX state occurs in two steps, suggesting that the initial system is somehow heterogeneous. (vii) The decay of the IMPX state is not complete when the system reaches the CTIST temperature upon warming.

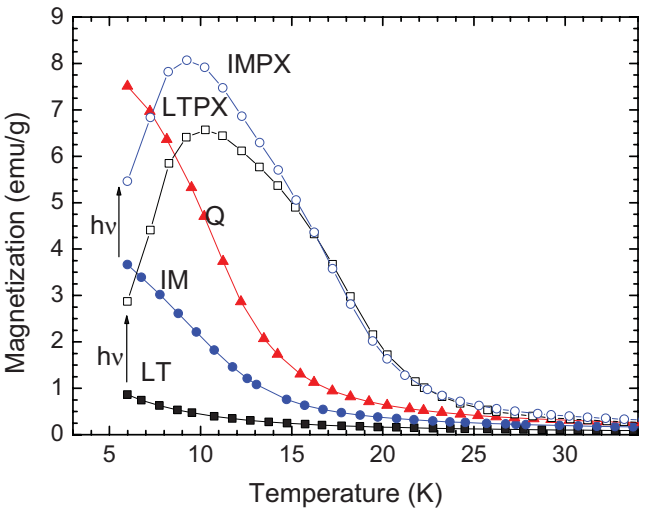


FIG. 2. (Color online) Low-temperature magnetization curves of the layer sample, recorded after rapid (Q state) or slow (IM state) cooling, or after photoexcitation (LTPX and IMPX states). The applied field was 0.1 T. The low-temperature increase of the LTPX and IMPX curves may be assigned to the nonrelaxed character of the raw photoinduced state of the system, which departs from the usual field-cooled state (Refs. 27 and 28). Magnetic freezing temperature values $T_C$ are listed in Table I.

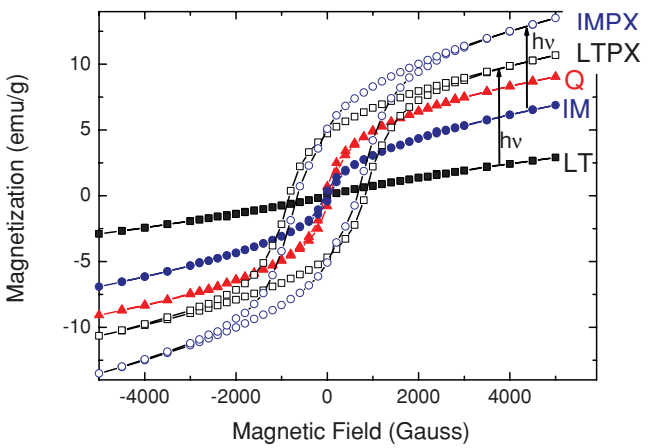


FIG. 3. (Color online) M-H curves measured at 6 K of the thin-layer sample.

TABLE I. Properties of the Q, LT, IM, LTPX, and IMPX states, derived from magnetic data. $T_C$ is the magnetic ordering (freezing) temperature determined as the inflection point of the low-temperature $M(T)$ curves. $T_{relax}$ is the thermal relaxation temperature determined as the inflection point of the $\chi_m \cdot T(T)$ curve during the thermal decay of the metastable state. $M_s$ is the zero-field extrapolated value of the $M(H)$ curves, with $B_c$ the coercive field. The low-temperature HS content was estimated by comparing the $\chi_m \cdot T$ values in the low-temperature plateau with those above the CTIST.

| State | $T_C$ (K) | $T_{relax}$ (K) | $M_s$ (emu/g) | $B_c$ (G) | HS content (%) |
|---|---|---|---|---|---|
| Q (bulk sample) | 14 | 160 | Not measured | Not measured | 85 |
| Q (layer sample) | 11 | 159 | 6.62 | 60 | 55 |
| LT | | | | ~0 | ~0 |
| IM (layer sample) | ~11 | | 4.00 | 60 | 25 |
| LTPX(layer sample) | 18 | 130–140 | 8.17 | 830 | ~50 |
| IMPX (layer sample) | 17 | 130,150–170 | 10.49 | 660 | ~60 |

*Magnetic properties of the Q and LTPX states*. It is worth considering the incomplete population of the HS state in the Q and LTPX states and its impact on the magnetic and relaxation properties. Due to the long lifetime of the PX states at low temperature, it must be considered that photoexcitation is a frontal process mainly limited by the bulk absorption of light in these highly colored samples. This leads to a nonhomogeneous state of the sample, with a front part almost saturated, leaving the part that is almost nonexcited.[3,4] The situation is quite different for the Q state, the incomplete character of which results from partial relaxation occurring at intermediate temperatures during the cooling process. In the case of a distribution of energy barriers, as reported for the Na analog,[20] relaxation proceeds faster with the switchable pairs having the lower energy barriers. Consequently, the final Q state preferably contains pairs having high-energy barriers. Such selectivity could slightly impact the thermal relaxation temperature,[29–31] but this effect is not reflected in the experimental data listed in Table I. Also, the magnetic ordering temperature is expected to be sensitive to the HS content, and indeed this effect is observed here (Table I).

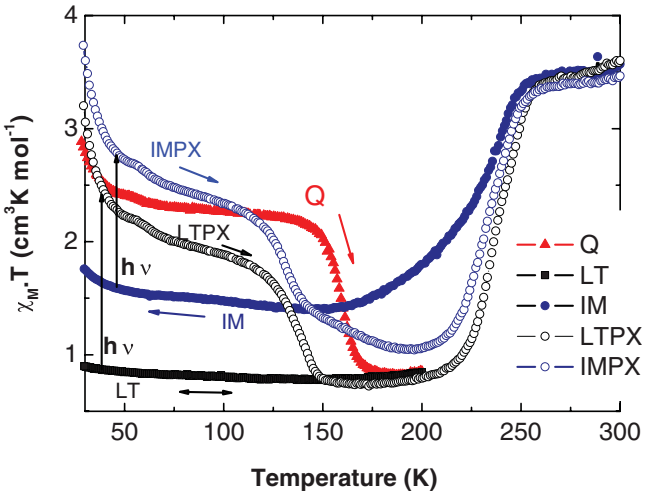


FIG. 4. (Color online) Temperature dependences of the $\chi_m \cdot T$ product obtained with the thin-layer sample under 0.1 T applied field. The photoexcited states were obtained after irradiation at 750 nm at 15 mW/cm$^2$ for 3 h, starting from the LT state (LTPX curve) or from the intermediate state (IMPX curve). Temperature scan rate was 1 K/min.

Using a rough linear extrapolation, which overestimates the result due to the usual shape of the magnetic dilution phase diagrams, we assign the value of $T_C \sim 15.5$ K to a hypothetical 100% quenched state. On the other hand, the $T_C$ value assigned to the LTPX state, $T_C \sim 18$ K, is certainly underestimated due to the incomplete transformation of the almost saturated fraction. Therefore, this analysis suggests a sizable difference between the $T_C$ values of the Q and LTPX states, below 16 K and above 18 K, respectively.

The present data for the Q and LTPX states qualitatively agree with the previous observations made for the Na compound.[10] The Q state possesses a lower $T_C$, a higher $T_{relax}$, and a smaller $M_s$ value for a comparable HS fraction. Also, according to the detailed structural investigation,[23] the unit-cell parameter has a smaller value in the Q state. The Q state is isostructural with the high-temperature phase (cubic, $Fm\bar{3}m$ space group), and a recent x-ray investigation[32] suggested that the LT phase has lower (rhombohedral) symmetry than the high-temperature phase. Following the textbook example of $Fe(ptz)_6$-based SC compounds,[33] it is generally assumed that photoexcitation at low temperature does not induce structural changes (although counterexamples seem to be provided by compounds possessing flexible ligands[29–31]). These two considerations led us to the simple idea that the decay of the Q state involves both electronic and structural transformations, while the decay of the LTPX state only involves an electronic transformation.

*Thermal decay of the Q and LTPX states*. In the experimental curves reported in Fig. 4, the difference in the thermal decay temperatures is assigned to the presence (Q state) or absence (LTPX state) of this structural transformation. This suggestion is supported by the fact that the decay temperature of the Q state does not sizably depend upon its HS content. The presence of a structural difference between the Q and LTPX states will also impact the isothermal relaxation curves reported below. It is also noteworthy that, during the low-temperature photoexcitation process, all lifetimes are long and there is no selectivity among states with different energy barriers. This absence of selection may contribute to the slight smearing of the thermal decay curve of the LTPX state.

*Nature of the IM state*. A crucial experimental feature is the two-step character of the decay of the IMPX state (see Fig. 4). These steps roughly coincide with the thermal return temperatures of the LTPX and Q states. It is therefore suggested that the IM state is a mixture of Q and LT-like

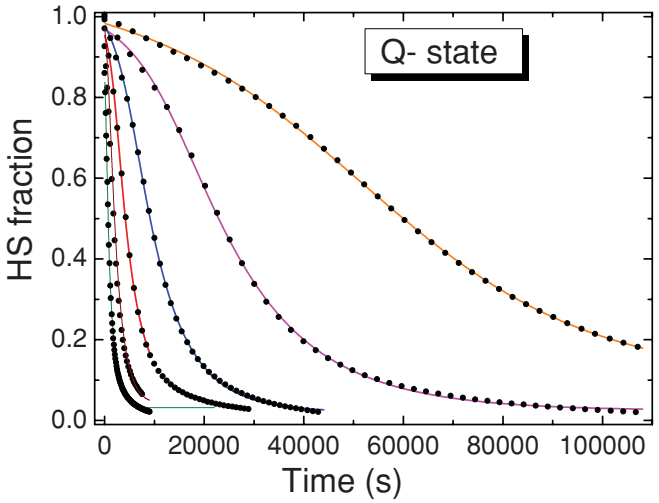


FIG. 5. (Color online) Isothermal relaxation curves for the Q state at 155, 150, 145, 140, 135, and 130 K, from left to right, with best-fit computed curves. The fitted parameters are given in Table II.

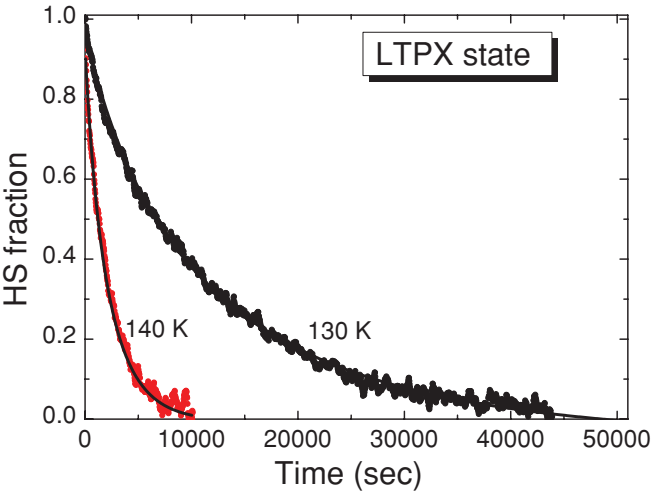


FIG. 6. (Color online) Isothermal relaxation curves for the LTPX state at 130 K and 140 K, with best-fit computed curves. The noise in the relaxation data, despite a preliminary smoothing over 10 neighboring values, is due to the very small sample mass used for the photomagnetic measurements. The fitted parameters are given in Table II.

fractions. This simple model is supported by the shapes of the $M(T)$ curve and $M$ versus $H$ loop of the IM state, which are strikingly similar to those of the partially relaxed thin-film-based Q state. Both experimental curves can be fairly well reproduced by linear combinations of the Q- and the LT-state data, in respective proportions 42 : 58 for the $M(T)$ curve and 62 : 38 for the $M(H)$ curve. These proportions lead to final estimates of the HS fraction in the IM state of 23% and 34%, which roughly agree with the magnetic data derived from Fig. 1 and listed in Table I. The difference between these estimates presumably results from the neglect of possible interactions between the Q-like and LT fractions.

It is worth noting that the second step of the decay of the IMPX state is smeared out over a broad temperature range, from ∼150 to ∼200 K. This effect can be assigned to local inhomogeneities, the nature of which will be discussed further below in the context of the diffraction data. At first glance, one might expect that IMPX should return to its initial IM state (LT + Q) after the first relaxation stage (LTPX → LT). However, the second stage, where the Q-type fraction relaxes, takes place more efficiently than for the initial IM state, an effect attributable to physical aging of the IM state.

*Isothermal relaxation of the Q and LTPX states.* The isothermal relaxation curves of the Q state, recorded with the bulk sample, are shown in Fig. 5. The data are normalized to the low-temperature value of the quenched HS fraction that is close to 1 at $t = 0$. The isothermal relaxation curves of the LTPX photoexcited state are shown in Fig. 6. These have been rescaled to the initial value of 1 for simplicity, as their almost single exponential character makes the parameters nearly independent of the scaling factor.

The shapes of the relaxation curves for the Q and LTPX states reveal qualitative differences since the Q-state curves exhibit a marked sigmoidal shape. However, both exhibit long relaxation tails, which usually can be assigned to distributions of relaxation times[34] or, alternatively, to the onset of correlations associated with short-range interactions.[35] To provide a further insight into these alternative assumptions, we apply here a model accounting for correlations.[36] We recall that the simple cooperative two-level relaxation model based on the mean-field approach, and using the Hauser self-acceleration factor[37] $k_{\rm HL}(T,n_{\rm HS}) = k_\infty \exp(-E_a^0/k_BT)\exp[-\alpha(T)n_{\rm HS}]$, where $\alpha = 2zJ/k_B$T, conveniently reproduces the sigmoidal shape of the relaxation curves until $n_{\rm HS} \sim 0.5$, but fails to overlap the long relaxation tails. As shown in Figs. 5, 6, and 14, these tails are accurately reproduced by the correlation model used here.

The two-variable correlation model of Ref. 36 is based on the pair approximation method, which includes short-range fluctuations of the $Co^{2+}$(HS)-$Fe^{3+}$ fractions by explicitly taking into account short-range correlations. The stochastic treatment of this problem yields two coupled differential equations governing the HS fractions $n_{\rm HS}(t)$ and the fraction of HS-LS pairs, denoted $n_{\rm HL}(t)$, where HS is representative of the $Co^{2+}$-$Fe^{3+}$ pairs and LS the $Co^{3+}$-$Fe^{2+}$ pairs. We show here, for simplicity, the shorter expressions suitable for the HS → LS relaxation process:

$$\frac{dn_{\rm HS}}{dt} = -\frac{n_{\rm HS}}{2\tau_0} e^{-\beta[E_a^0 + J(2n_{\rm HS}-1) - \Delta + \frac{1}{2}k_BT\ln(g)]} \times \left(e^{-\beta J_{\rm short}} + 2\frac{n_{\rm HL}}{n_{\rm HS}}\sinh(\beta J_{\rm short})\right)^q \quad (1)$$

and

$$\frac{dn_{\rm HL}}{dt} = -\frac{n_{\rm HS}}{2\tau_0} e^{-\beta[E_a^0 + J(2n_{\rm HS}-1) - \Delta + \frac{1}{2}k_BT\ln(g)]} \times \left(e^{-\beta J_{\rm short}} + 2\frac{n_{\rm HL}}{n_{\rm HS}}\cosh(\beta J_{\rm short})\right) \times \left(e^{-\beta J_{\rm short}} + 2\frac{n_{\rm HL}}{n_{\rm HS}}\sinh(\beta J_{\rm short})\right)^{q-1} \quad (2)$$

TABLE II. Refined parameters for the isothermal relaxation curves of $K_{0.3}Co[Fe(CN)_6]_{0.74} \cdot 3.4H_2O$ shown in Figs. 5 (Q state) and 6 (LTPX state) using the two-variable correlation model (Ref. 36) (due to the tight correlation between $E_a$ and $\tau_0$ parameters, the fixed value $E_a = 5000$ K was used to make $\tau_0$ values essentially independent of temperature. The crude choice of $E_a$ has no impact on the other parameters). Underlined values were fixed during the fit.

| State | $T$ (K) | $1/\tau_0$ ($s^{-1}$) | $J$ (K) | $J_{short}$ (K) | Scaling factor | HS residual |
|---|---|---|---|---|---|---|
| Q | 130 | $0.246 \times 10^{11}$ | −2.1 | 64.9 | 0.853 | 0.135 |
| | 135 | $0.301 \times 10^{11}$ | −57.2 | 105 | 0.946 | 0.024 |
| | 140 | $0.276 \times 10^{11}$ | −72.7 | 109 | 0.954 | 0.021 |
| | 145 | $0.289 \times 10^{11}$ | −88.1 | 127 | 0.919 | 0.032 |
| | 150 | $0.203 \times 10^{11}$ | −84.8 | 114 | 0.910 | 0.052 |
| LTPX | 130 | $0.539 \times 10^{11}$ | −55.4 | 0 | 1.02 | −0.05 |
| | 130 | $0.551 \times 10^{11}$ | 0 | −12.1 | 1.01 | −0.04 |
| | 140 | $0.436 \times 10^{11}$ | −26.7 | 0 | 0.93 | 0.07 |
| | 140 | $0.438 \times 10^{11}$ | 0 | −6.2 | 0.93 | 0.07 |

with $\beta = 1/k_B T$ and $J$ and $J_{short}$ are the long- and short-range interaction parameters, taken as temperature independent for simplicity; $q$ is the connectivity of the system, taken equal to 4 considering the partial occupancy (0.77) of the Fe sites in the 3D lattice and accounting for (unpublished) Mössbauer data, which show that only ~80–90% of the iron atoms participate in the charge-transfer process. $E_a^0$ (noted $E_a$ in the following) is the activation energy of the symmetrical double-well system and the frequency factor $1/\tau_0$ is equivalent to $k_\infty$ (given in Hauser equation). $2\Delta$ is the energy gap and $g$ is the effective degeneracy ratio of the HS and LS states, determined from calorimetric measurements as $\ln g = \Delta S/R$, where $R$ is the gas constant. When the above equations are completed with the LS → HS process, the model also provides the quasistatic behavior of the system at the thermal transition. Fits to the relaxation curves based on the above equations are shown in Figs. 5, 6, and 14, and the fitting parameters are listed in Table II. To get better agreement, we also introduced a multiplicative scaling factor and a residual value of the HS fraction, which mainly compensate for minor errors of the normalization procedure of the experimental data. The fitted data reveal an unexpected thermal variation, which will be addressed in the discussion section in the light of the relaxation data obtained with the Na analog.

The values of $E_a$ and $\tau_0$ were determined by refining an Arrhenius plot of the values obtained at different temperatures for the frequency factor $(1/\tau_0)\exp(-E_a/k_B T)$. We obtained $E_a = 4850$ (200) K, with the frequency factor $\ln(1/\tau_0) = 23.(2)$ leading to $1/\tau_0 \sim 1.0 \times 10^{10}$ $s^{-1}$. It is worth remembering that the barrier selectivity associated with the quenching process is expected to slightly overestimate the frequency factors, and the data for the PX state lead to slightly smaller values $E_a = 4610$ K and $1/\tau_0 \sim 2.8 \times 10^9$ $s^{-1}$.

The data derived from the relaxation of the Q state reproduce the CTIST properties rather well, as shown in Fig. 7 (curve Q). The problem of the quantitative consistency between the relaxation and thermal transition data previously addressed[20] seems to have a minor impact here. The quasiexponential relaxation data of the LTPX state does not lead to a

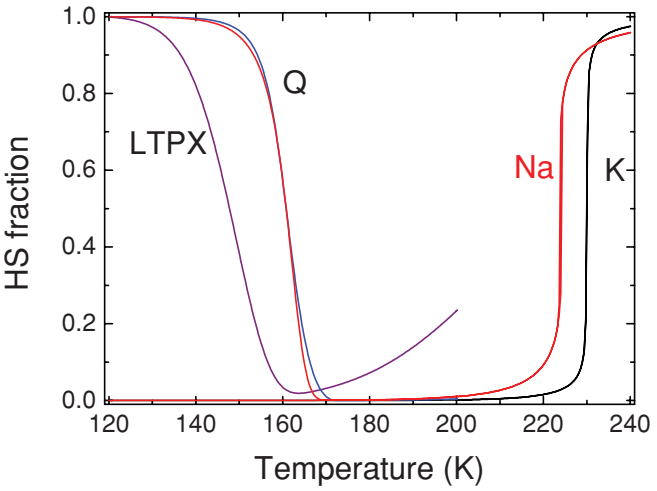


FIG. 7. (Color online) Computed thermal relaxation and thermal transition curves of the K compound, using kinetic and interaction parameters derived from the analysis of the relaxation curves (black full lines). The red line corresponds to the Na-analog data. The energy gap values have been determined (3450 and 2688 K for the K and Na compounds, respectively) so as to match the experimental transition temperature ranges.

cooperative thermal transition. For the needs of the coming discussion, we also present in Fig. 7 the transition curve computed in a similar way, that is, using the relaxation data of the Q state, for the Na analog, which does not reproduce the ~20-K-wide experimental hysteresis.

Finally, we briefly address the problem of the energy barrier distributions. In previous work[20] using a spin-crossover compound,[29–31] we demonstrated that ligand field distributions efficiently compete against the interaction parameters, and reduce the effective cooperativity of the system, manifested in the sigmoidal character of the relaxation curves and the width of the thermal hysteresis loop. As for the Na analog, a distribution of energy gaps can be assigned to different $CoN_{6-x}O_x$ environments known to exist in the K compound, associated with the change in ligand field strength on $H_2O$ substitution and possible local distortions generated by the random occupancy of the $Fe(CN)_6$ sites. However, these distributions are also present in the Q state and would hardly explain the striking difference between the relaxation of the Q and LTPX states. Instead, we assign this difference to the structural change, which occurs during the decay of the Q state.

### B. Calorimetric data

DSC measurements at 1 K/min upon cooling from room temperature and subsequent heating are reported in Fig. 8. They refer to the HT ↔ IM transformation and show atypical features. The $C_p$ anomaly on cooling is significantly smaller than the one on heating, and below the temperature of the anomaly, the slope of the cooling branch is much different from that of the heating branch. These features agree with the nonequilibrium character of the HT ↔ IM transformation as suggested by the kinetic effects seen in Fig. 1. Also, the cooling curve is single peaked, while the heating branch appears doubly stepped. The data obtained starting from the quenched sample is reported in Fig. 9. The decay of the Q state

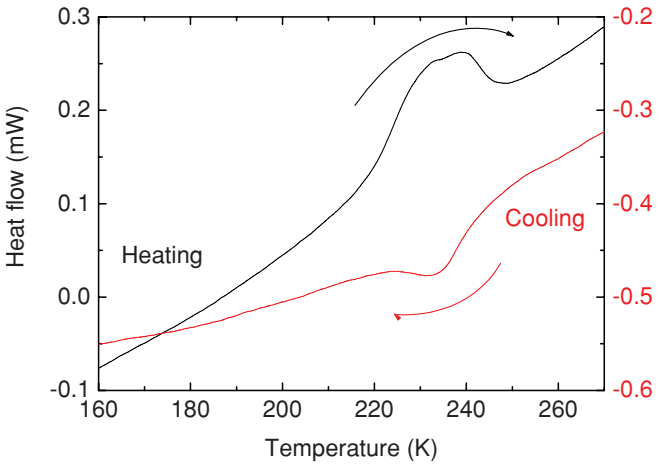


FIG. 8. (Color online) DSC measurements performed at 1 K/min: cooling from room temperature and subsequent heating, associated with the HT ↔ IM transformation.

is also single peaked, but the peak of the LT → HT transition is again multistepped. The quantitative data are summarized in Table III and reveal that the ΔH of the IM → HT transformation is roughly half of that measured at the LT → HT transition, which is consistent with the description of the IM state in terms of a nearly equal mixture of Q and LT states. Also, ΔH of the Q → LT transformation is much less than for the LT → HT transition, due to the incomplete character of the quenching process (∼50% yield). The $C_p$ peak on heating occurs at ∼160 K, which agrees with the value ∼159–160 K determined by magnetic measurements at the same scan rate.

The complex shapes of the $C_p$ anomalies of the LT → HT and IM → HT transitions agree with the idea that multiscale processes take place involving both electronic and structural transformations, and that other factors are also at play, such as internal stresses created by the large volume change upon the CTIST transition ($\Delta V/V$ ∼9%). However, the Q → LT transformation, which also involves both processes, does

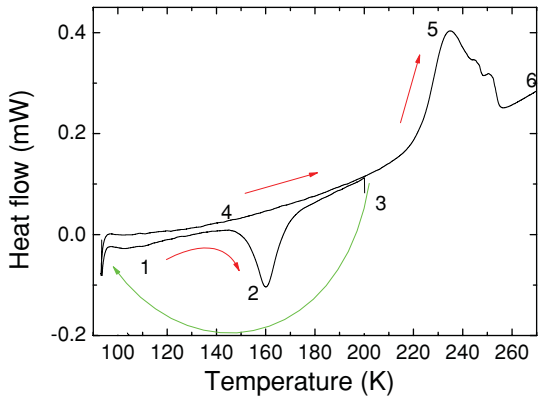


FIG. 9. (Color online) DSC measurements performed at 1 K/min: starting from externally quenched sample, associated with the Q → LT (1 to 3) and LT → HT (4 to 6) transformations.

TABLE III. Characteristic temperatures ($T_m$), enthalpy (ΔH), and entropy (ΔS) values determined from the calorimetric measurements corresponding to the CTIST (IM ↔ HT and LT ↔ HT) and relaxation (Q → LT) transitions. [The starred value ΔS (Q → LT) includes entropy creation due to irreversibility.]

| | HT → IM | IM → HT | Q → LT | LT → HT |
|---|---|---|---|---|
| $T_m$ (K) | 230 | 230–235 | 160 | 235 |
| ΔH (kJ mol$^{-1}$) | ≈3 | 8.7 | 7.1 | 18.0 |
| ΔS (J mol$^{-1}$ K$^{-1}$) | ≈13 | 37.3 | 44.5(⋆) | 76.2 |

not result in such a complex shape of the $C_p$ anomaly. We imagine that the various factors involved in these two kinds of solid-state transformations may differ due to the different temperatures at which these transformations take place. Also, the impact of defects that can hinder electron transfer may depend upon temperature.

According to Table III, the measured ΔH and ΔS values for the LT → HT transition are ∼25% larger than for the Na analog, despite a similar proportion of active Co-Fe switchable pairs (∼80% in both cases according to the Mössbauer data). This presumably results from a larger contribution of the structural processes. As in previous work,[21] we determined the entropy change associated with the complete switching of a mole of Co-Fe pairs as ΔS(corrected) = ΔS(measured)/0.77/0.8 ∼ 125 JK$^{-1}$ mol$^{-1}$ per mole, leading to the degeneracy factor value $\ln(g) = \Delta S/R \sim 15$ to be used in the Ising model calculations. Accordingly, the value of the electronic gap in the model may be derived from the ΔH value reported to one mole of switchable pairs $2\Delta \sim \Delta H(\text{corrected})/N = 3510$ K, where $N$ is the Avogadro number.

### C. Diffuse reflectance

The powder sample was initially cooled within a few hours in the dark down to 80 K and then irradiated overnight at 750 nm. We then recorded the diffused intensity under constant irradiation for temperature sweeps up to room temperature and then back to 80 K, at scan rates close to 0.2 K/min (Fig. 10). The data reveal striking features: (i) a drastic reduction of the kinetic effect associated with the onset of the IM state; (ii) the presence of a light-induced thermal hysteresis[14,38,39] (LITH) at lower temperature, revealing that cooperative relaxation efficiently competes against photoexcitation; and (iii) the coincidence of the heating and cooling branches in the plateau temperature interval (150–200 K). It should be kept in mind that we previously concluded that the LT state was obtained after the decay of both IMPX and LTPX states. Consequently, the heating branch of the plateau has to be assigned to the LT state. However, it overlaps the cooling branch, which was expected to be in the IM state. To elucidate the possible role of light in these experiments, we performed snapshot measurements that minimize the impact of light on the photoswitchable samples (Fig. 11). We compared two sets of data, on cooling, starting from either the HT or from the LT state. It is shown that cooling in the dark from the HT state effectively induces the IM state, although the difference with the LT state is smaller than expected from the magnetic measurements.

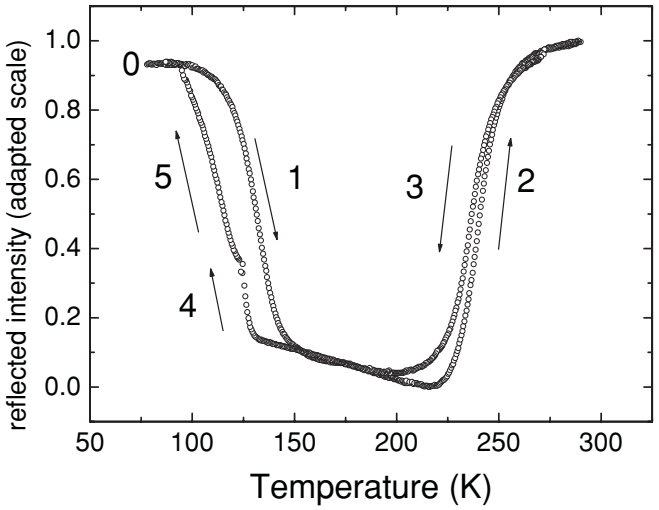


FIG. 10. Diffuse reflectance data under constant irradiation, obtained after photoexcitation overnight at 80 K. Effective scan rates were 0.18, 0.25, 0.20, 0.004, and 0.18 K/min for sections 1 to 5, respectively.

Due to the small difference in reflectance observed for the IM state in the dark and the plateau values in Fig. 11, we suggest that light may hinder the onset of the IM state. Also, the reduction of the kinetic hysteresis of the thermal transition, relative to the magnetic measurements in the dark, might reveal a light-induced acceleration of the HT → LT relaxation, a point that is addressed further in the discussion section.

### D. X-ray diffraction data

We focus here on the properties of the IM state. A more complete structural analysis of the multistable states will be reported separately.[23] Figure 12 shows a typical diffraction

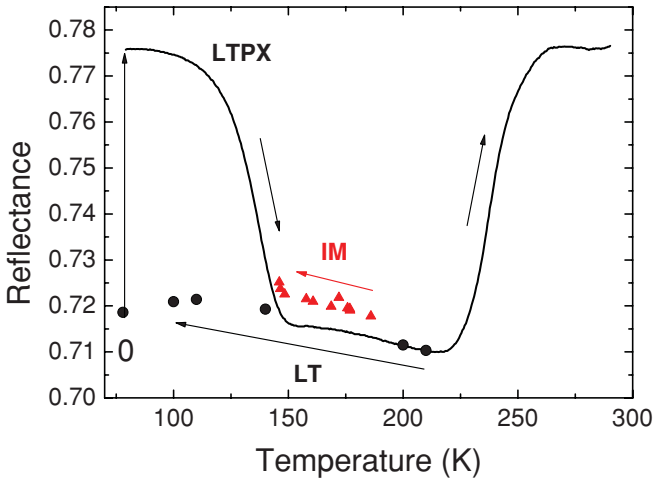


FIG. 11. (Color online) Reflectance data obtained as snapshots under slow cooling from the HT state to generate the IM state (full triangles) or after relaxation of the PX state in the dark to generate the LT state (full circles). Both data sets are obtained on cooling. The data recorded under permanent light are shown for comparison (full line). Note that the snapshots around 200 K after relaxation in the dark accurately match the full line.

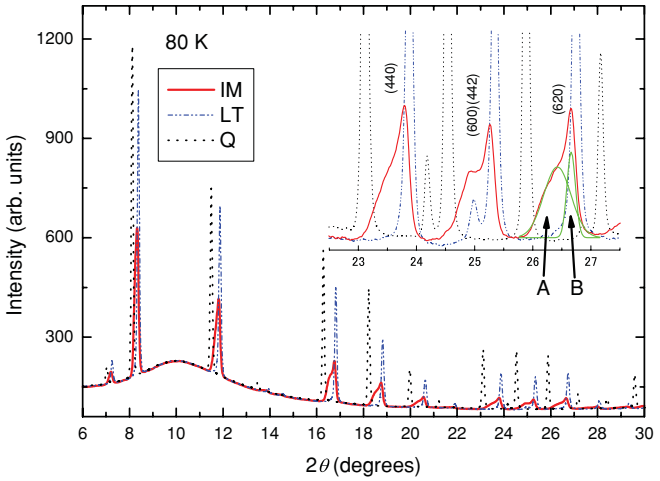


FIG. 12. (Color online) X-ray diffraction pattern of the K compound at 80 K in the cooling branch of the IM state, with comparison to those of the LT and Q states. Inset: Zoom of the most resolved lines, with analysis into Gaussian doublets ($A$ = broad, $B$ = narrow).

pattern of the IM state, taken at 80 K on cooling. The IM lines are split into a broad component, here labeled IM-A and a narrow component, IM-B, establishing the biphasic character of the IM state. The observed phase separation is specific to the slowly cooled IM state, and it is worth noting that all other states, except the IMPX state, exhibit a single pattern with narrow lines, typical for homogeneous single-phase materials. The lattice parameter of the broad component IM-A is 10.095 Å, corresponding to a ∼48 : 52 mixture of HS and LS states, based on the Q state (10.263 Å at 80 K) and LT state (9.937 Å at 80K) parameters, whearas the narrow peak labeled IM-B corresponds to a lattice constant of 9.979 Å, which is close to that of the LS state. The diffraction data unambiguously assign the A and B fractions to the partially relaxed Q (with ∼50% HS fraction) and LT states, as already suggested by the magnetic data. The broad character of the IM-A lines results from a distribution of HS and LS sites in this phase. The slight increase of the lattice parameter values of the IM-B lines with respect to the pure LT state can be attributed to elastic interactions between microphases. The Q : LT proportions are ∼60 : 40, in rough agreement with the magnetic data. It is important to note here that the HS content of the Q state, as well as the composition of the IM state, sensitively depends on the cooling rate, and may differ between the x-ray experiment, which employs faster cooling, and the photomagnetic experiments.

In a further step, we systematically analyzed the patterns using Gaussian lineshapes and interpreted the data using the Stokes and Wilson formula:[40,41] $[\beta\cos(\theta)]^2 = [2\eta\sin(\theta)]^2 + (\lambda/\epsilon)^2$, where $\beta$ and $2\theta$ are the width and positions of the diffraction lines, and $\eta$ and $\epsilon$ are the heterogeneity ratio and coherence length value. The unknown parameters $\eta$ and $\epsilon$ are determined by linear regression of the experimental plots of $\beta\cos(\theta)$ versus $\sin(\theta)$. The peak broadening is given by $\beta^2 = \beta_{\text{exp}}^2 - \beta_0^2$, where $\beta_{\text{exp}}$ and $\beta_0$ are the experimental peak widths and those of a reference sample ($LaB_6$ NIST standard) averaged over the same $\theta$ interval. The resulting values are reported in Fig. 13, together with the variations of the lattice parameters and the proportions of the A and B components.

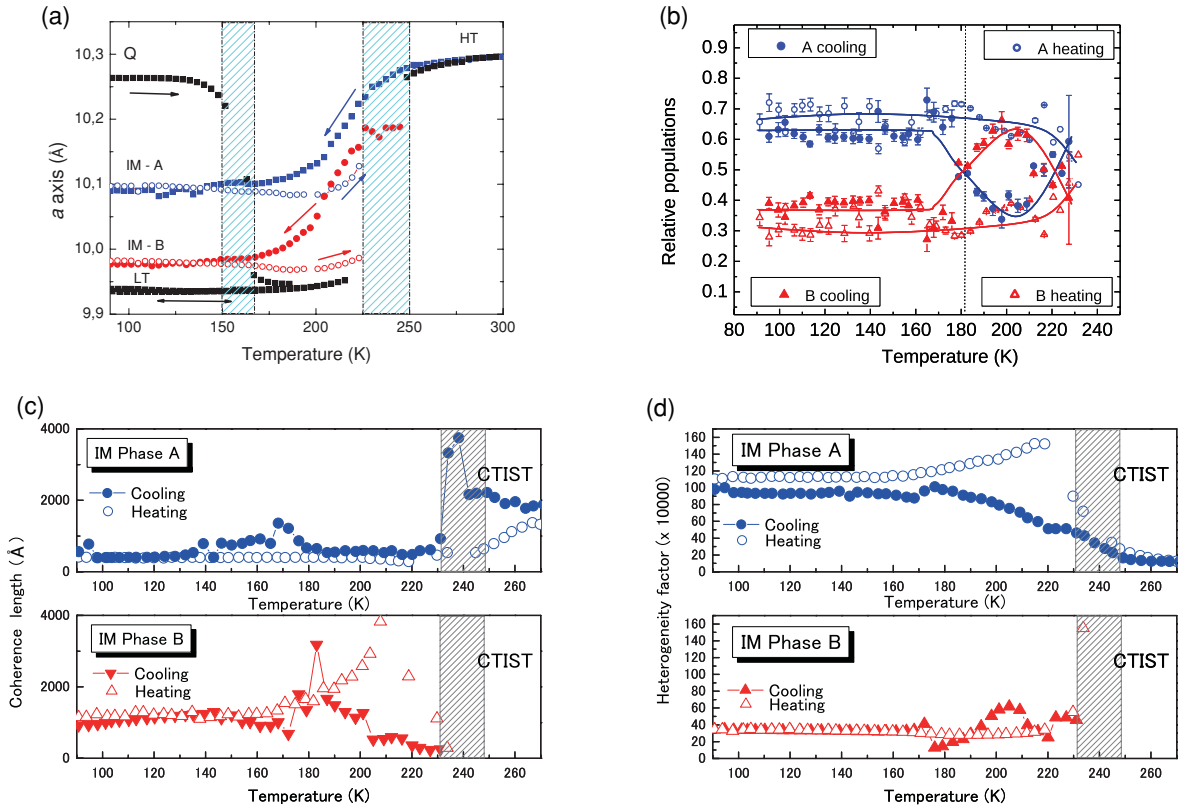


FIG. 13. (Color online) Structural data of the IM phase during thermal cycling: (a) temperature dependence of the lattice parameter value in Q, IM-*A*, IM-*B*, LT, and HT phases; (b), (c), (d) temperature dependence of the relative population (b), coherence length (c), and heterogeneity factor (d) of the IM-*A* (circles) and IM-*B* (triangles) states determined by application of the Stokes and Wilson formula. Solid (open) symbols stand for cooling (heating) runs.

The IM-A phase has a coherence length of ∼50 nm at 180 K, corresponding to ∼50 unit cells and is more clusterlike than the IM-B phase, with a coherence length of ∼200 nm through the whole temperature range. The former values compare to those previously reported upon rapid cooling of the sodium analog $Na_{0.42}Co[Fe(CN)_6]_{0.78} \cdot 4.64H_2O$, which were observed to be in the range 10–50 nm.[42]

## IV. DISCUSSION

### A. Comparison to the Na analog (relaxation properties)

First, we show the relaxation data of the Na analog, in Fig. 14, with best-fitted curves using the same model as that applied to the K analog. The agreement with the experimental data is excellent, even to long times. The fitting parameters are listed in Table IV. An Arrhenius plot leads to $E_a = 4600$ (70) K and $k_\infty = 1/\tau_0 \sim 1.0 \times 10^9\ s^{-1}$ and a barrier energy of $E_{HL}(n_{HS} = 1/2) = E_a - \Delta \sim 3260$ K in fair agreement with the value ∼3420 K reported by the previous analysis using a mean-field model based on a distribution of relaxation times.[20]

Using these parameters, we computed the transition curves for the Na analog shown in Fig. 7, but failed to reproduce the 20-K-wide experimental hysteresis. A possible explanation is based on the structural data reported in Ref. 10, which shows that the Q state undergoes an electronic relaxation toward a Q-relaxed state prior to the structural relaxation toward the LT state. The cooperativity associated with this latter transformation is missing during the electronic transformation observed by magnetic measurements. This explanation does not exclude the presence of distributions effects as assumed in

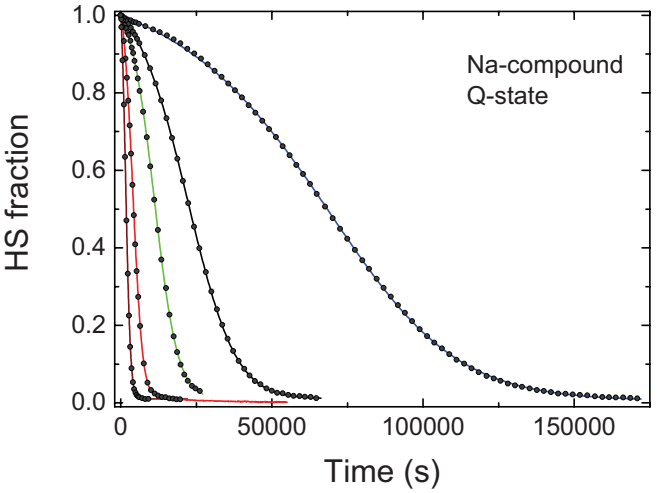


FIG. 14. (Color online) Isothermal relaxation curves for the Q state of $Na_{0.32}Co[Fe(CN)_6]_{0.74} \cdot 3.4H_2O$ at 150, 145, 140, 135, and 130 K, left to right, adapted from Ref. 20 with best-fit computed curves using the present model. The fitting parameters are given in Table IV.

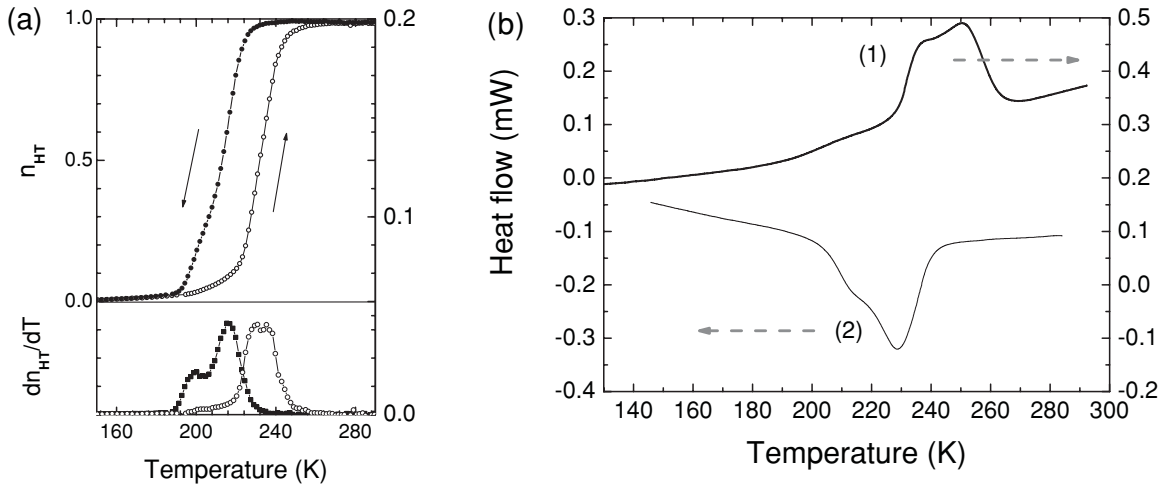


FIG. 15. Thermal transition hysteresis loop of $Na_{0.32}Co[Fe(CN)_6]_{0.74} \cdot 3.4H_2O$, from magnetic measurements (a) and from calorimetric measurements (b). Adapted from Refs. 20 and 21, respectively.

Ref. 20, but they probably act to a lower extent since they are expected to be similar in the two analogous compounds.

### B. On the multistep character of the thermal transition

The two-step character of the IMPX → LT relaxation, and of the HT → IM and LT → HT transformations of the K compound, was mentioned in the previous sections. A detailed inspection of the thermal transition in the Na analog reveals a similar double-step character (Fig. 15). It is worth noting that the shape of the thermal loop in the magnetic data of the Na compound is reminiscent of the kinetic distortion due to the onset of the IM state in the K compound. The multistep character of the $C_p$ anomaly at the LT → HT transformation of the K compound (Fig. 9) shows that this transformation is more complex than the simple succession of an electronic and a structural process.

### C. The interaction parameter values

We turn now to a detailed inspection of the interaction parameters for the Q state of the K and Na analogs (Tables II and IV). The two compounds exhibit similar values of the short-range parameter, but very different values of the long-range parameter, which is close to zero in the Na analog and mainly large and negative in the K compound. In addition, the data for the K compound exhibit large thermal dependences for both parameters, with some degree of correlation between them, while those of the Na analog remain almost temperature independent. We think that these different features result from the different natures of the processes. The complex behavior of the Q state of the K compound should be associated with the twofold aspect of the process, electronic and structural, which in principle should involve two order parameters. It is conceivable that these two order parameters are governed by different activation energies and/or time scales and may result in a sizable temperature dependence of the average parameters presently used. Conversely, the approximate temperature independence of the fitted data for the Na analog suggests a relaxation process governed by a single order parameter that is electronic in nature. An alternative explanation might arise from the elastic nature of the interaction parameters, possibly leading to sizable thermal variations. Such is the case in the spin-Peierls transition,[43,44] for example, in which the exchange interaction is modulated by the gradual dimerization of the lattice. Another important point is the opposite signs obtained for the short- and long-range interactions in the K compound. It is well known that the presence of opposite interactions may lead to cluster formation, although whether or not this peculiarity is correlated to the creation of the IM state remains an open question.

TABLE IV. Refined parameter values for the isothermal relaxation curves of the Q state of $Na_{0.32}Co[Fe(CN)_6]_{0.74} \cdot 3.4H_2O$ shown in Fig. 14, using the correlation model with fixed value $E_a = 5000$ K.

| State | $T$ (K) | $1/\tau_0$ ($s^{-1}$) | $J$ (K) | $J_{short}$ (K) | Scaling factor | HS residual |
|---|---|---|---|---|---|---|
| Q | 130 | $0.262 \times 10^{11}$ | 11.8 | 78.0 | 0.995 | 0.006 |
| | 135 | $0.236 \times 10^{11}$ | 3.6 | 73.9 | 0.994 | 0.010 |
| | 140 | $0.209 \times 10^{11}$ | 2.3 | 86.7 | 0.991 | 0.010 |
| | 145 | $0.205 \times 10^{11}$ | −10.7 | 86.1 | 0.991 | 0.013 |
| | 150 | $0.165 \times 10^{11}$ | −26.2 | 77.9 | 0.993 | 0.012 |

### D. On the possible origin of the IM state

We now discuss the physical properties of the IM state. The kinetic onset of the IM state and its short-range character imply a self-organization process. The driving force for this onset presumably originates from elastic stresses that are associated with the volume change upon the CTIST transformation. The short coherence length of the IM-*A* phase suggests the presence of strongly inhomogeneous stresses, which compete against the cooperative character of the transition. These stresses finally result in a smooth transformation over a

wide temperature range, yielding a slow relaxation regime upon cooling before the CTIST is completed. A similar effect of internal stresses upon a spin transition was recently illustrated in the spin-crossover compound $Fe(bbtr)_3(ClO_4)_2$ using optical microscopy. The inhomogeneous character of the transition in large crystals, due to the presence of internal stresses, resulted in large shifts ($\sim -20$ K) of the transition temperature in the stressed regions of the material.[45,46] Such a stress-based mechanism was able to explain the impact of the sample's thermal history upon the spin transition temperature.[47]

The self-organization process giving rise to the IM state certainly derives from elastic stresses resulting from the volume change associated with the CTIST process. We suggest that the growth of the IM state is a key factor affecting the stabilization of the quenched component, which would normally rapidly relax to the stable LT state, as it does in the Na compound and other photomagnetic Prussian blue analogs. The onset of the microstructure presumably induces stresses that slow down the relaxation of the Q state. The coupling between the electronic and structural transformations involved in the CTIST process may also take part in this complex mechanism. Finally, as suggested by diffuse reflectance data, the self-organization process may be hindered by illumination, which is expected to randomize the distribution of HS and LS states in the lattice.

## V. SUMMARY AND CONCLUSION

The unusual properties of the intermediate (IM) state obtained by slow cooling of the photomagnetic Prussian blue analog $K_{0.3}Co[Fe(CN)_6]_{0.77} \cdot 3.6H_2O$ have been described, while characterizing the magnetic properties of the different low-temperature states, including the quenched (Q), slow-cooled (IM), and low-temperature (LT) states, along with the corresponding photoexcited states LTPX and IMPX. From the relaxation properties of the metastable Q, LTPX, and IMPX states, it is inferred that the IM state is a mixture of the Q-type and LT phases. This conclusion is confirmed by x-ray diffraction. Further investigations show the fragile character of the IM state with respect to fatigue and irradiation by visible light. Calorimetric data support the complex character of the thermal transition, which was previously observed for the $Na_{0.32}Co[Fe(CN)_6]_{0.74} \cdot 3.4H_2O$ analog. For both compounds, the relaxation curves have been analyzed using a two-variable correlation model, which nicely predicts the experimental data. On the other hand, whereas the model reproduces the thermal hysteresis of the Na compound, the agreement is less for the K analog, further illustrating the complex character of the transformations in the title compound. The origin of the IM state is attributed to a self-organization process, and a complete structural investigation of the system will be reported separately.

## ACKNOWLEDGMENTS

This work was supported by CNRS, Versailles University, Région Ile-de-France, Projects No. MAT2007-61621 and No. CSD2007-00010 from the Spanish Ministerio de Educación y Ciencia and FEDER, and European Union Network of Excellence MAGMANet (Contract No. NMP3-CT-2005-515767-2) and partially supported by the US National Science Foundation through Grant Nos. DMR-0453362 and DMR-1005581 (DRT). The authors thank Professor M. W. Meisel for insights, J. H. Park for early contributions to this work, and M. Andrus for verifying the chemical analysis.

*Present address: Laboratoire d'Ingénierie des Systèmes de Versailles (LISV), Université de Versailles Saint-Quentin, 45 Avenue des Etats-Unis, 78035 Versailles, France.

†Present address: Division of Physics, Institute of Liberal Education, Nihon University School of Medecine, Oyaguchi Kamicyo 30-1, Itabashi 173-8010, Japan.

‡kbo@physique.uvsq.fr

§Present address: Faculty of Electrical Engineering and Computer Science, Stefan cel Mare University, Suceava 720229, Romania.

‖varret_francois@yahoo.fr

[1] S. Ferlay, T. Mallah, R. Ouahs, P. Veillet, and M. Verdaguer, Nature (London) **378**, 6558 (1995).

[2] O. Sato, T. Iyoda, A. Fujishima, and K. Hashimoto, Science **272**, 704 (1996).

[3] F. Varret, A. Goujon, J. Jeftic, M. Noguès, A. Bousseksou, S. Klokishner, A. Dolbecq, and M. Verdaguer, Hyperfine Interact. **113**, 37 (1998).

[4] F. Varret, M. Noguèś, and A. Goujon, *Magnetism: Molecules to Materials*, edited by J. Miller and M. Drillon (Wiley-VCH, Weinheim, 2001), Chap. 2, p. 257.

[5] P. Gütlich, Y. Garcia, and T. Woike, Coord. Chem. Rev. **219-221**, 839 (2001).

[6] M. Soraï, Bull. Chem. Soc. Jpn. **74**, 2223 (2001).

[7] F. Varret, K. Boukheddaden, E. Codjovi, and A. Goujon, Hyperfine Interact. **165**, 37 (2005).

[8] T. Yokoyama, T. Ohta, O. Sato, and K. Hashimoto, Phys. Rev. B **58**, 8257 (1998).

[9] T. Yokoyama, M. Kiguchi, T. Ohta, O. Sato, Y. Einaga, and K. Hashimoto, Phys. Rev. B **60**, 9340 (1999).

[10] I. Maurin, D. Chernyshov, F. Varret, A. Bleuzen, H. Tokoro, K. Hashimoto, and S. I. Ohkoshi, Phys. Rev. B **79**, 064420 (2009).

[11] T. Yamauchi, A. Nakamura, Y. Moritomo, T. Hozumi, K. Hashimoto, and S. Okhoshi, Phys. Rev. B **72**, 214425 (2005).

[12] Y. Moritomo, F. Nakada, H. Kamioka, T. Hozumi, and S. Ohkoshi, Phys. Rev. B **75**, 214110 (2007).

[13] V. Escax, A. Bleuzen, C. C. dit Moulin, F. Villain, A. Goujon, F. Varret, and M. Verdaguer, J. Am. Chem. Soc. **123**, 12536 (2001).

[14] J.-F. Letard, P. Guionneau, L. Rabardel, J. A. K. Howard, A. E. Goeta, D. Chasseau, and O. Kahn, Inorg. Chem. (Washington, DC) **37**, 4432 (1998).

[15] J. S. Costa, P. Guionneau, and J.-F. Létard, J. Phys: Conf. Series **21**, 67 (2005).

[16] O. Sato, Y. Einaga, T. Iyoda, A. Fujishima, and K. Hashimoto, J. Electrochem. Soc. **144**, L11 (1997).

[17] A. Goujon, O. Roubeau, M. Noguès, F. Varret, A. Dolbecq, and M. Verdaguer, Eur. Phys. J. B **14**, 115 (2000).
[18] A. Bleuzen, C. Lomenech, V. Escax, F. Villain, F. Varret, C. C. dit Moulin, and M. Verdaguer, J. Am. Chem. Soc. **122**, 6648 (2000).
[19] D. A. Pejakovic, J. L. Manson, J. S. Miller, and A. J. Epstein, Synth. Met. **122**, 529 (2001).
[20] S. Gawali, F. Varret, I. Maurin, C. Enachescu, M. Malarova, K. Boukheddaden, E. Codjovi, H. Tokoro, S. Ohkoshi, and K. Hashimoto, J. Phys. Chem. B **109**, 8251 (2005).
[21] M. Castro, J. Rodríguez-Velamazán, K. Boukheddaden, F. Varret, H. Tokoro, and S. Ohkoshi, Europhys. Lett. **79**, 27007 (2007).
[22] J.-H. Park, F. Frye, N. E. Anderson, D. M. Pajerowski, Y. D. Huh, D. R. Talham, and M. W. Meisel, J. Magn. Magn. Mater. **310**, 1458 (2007).
[23] M. Itoi (unpublished).
[24] C. Enachescu, F. Varret, E. Codjovi, J. Linarès, S. Floquet, P. Manikandan, and P. Manoharan, J. Phys. Chem. B **110**, 5883 (2006).
[25] C. J. O'Connor, Prog. Inorg. Chem. **29**, 203 (1982).
[26] W. Morscheidt, E. Codjovi, J. Jeftic, J. Linarès, A. Bousseksou, H. Constant-Machado, and F. Varret, Meas. Sci. Technol. **9**, 1311 (1998).
[27] A. Goujon, F. Varret, V. Escax, A. Bleuzen, and M. Verdaguer, Polyhedron **20**, 1347 (2001).
[28] F. Varret, A. Goujon, and A. Bleuzen, Hyperfine Interact. **134**, 69 (2001).
[29] V. Mishra, R. Mukherjee, J. Linares, C. Balde, C. Desplanches, J. Létard, E. Collet, L. Toupet, M. Castro, and F. Varret, Inorg. Chem. **47**, 7577 (2008).
[30] H. Mishra, V. Mishra, F. Varret, R. Mukherjee, C. Balde, C. Desplanches, and J.-F. Létard, Polyhedron **28**, 1678 (2009).
[31] V. Mishra, H. Mishra, R. Mukherjee, E. Codjovi, J. Linarès, J.-F. Létard, C. Desplanches, C. Baldé, C. Enachescu, and F. Varret, Dalton Trans. **36**, 7462 (2009).
[32] A. Bleuzen, J.-D. Cafun, A. Bachschmidt, M. Verdaguer, P. Munsch, F. Baudelet, and J.-P. Itie, J. Phys. Chem. C **112**, 17709 (2008).
[33] L. H. Böttger, A. I. Chumakov, C. M. Grunert, P. Gütlich, J. Kusz, H. Paulsen, U. Ponkratz, V. Rusanov, A. X. Trauwein, and J. A. Wolny, Chem. Phys. Lett. **429**, 189 (2006).
[34] A. Hauser, J. Alder, and P. Gütlich, Chem. Phys. Lett. **152**, 468 (1988).
[35] H. Romstedt, H. Spiering, and P. Gütlich, J. Phys. Chem. Solids **59**, 1353 (1998).
[36] B. Hôo, K. Boukheddaden, and F. Varret, Eur. Phys. J. B **17**, 449 (2000); see also K. Boukheddaden, F. Varret, A. Salunke, J. Linares, and E. Codjovi, Phase Transitions **75**, 733 (2002).
[37] A. Hauser, J. Jeftic, H. Romstedt, R. Hinek, and H. Spiering, Coord. Chem. Rev. **190-192**, 471 (1999).
[38] A. Desaix, O. Roubeau, J. Jeftic, J. G. Haasnoot, K. Boukheddaden, E. Codjovi, J. Linares, M. Nogues, and F. Varret, Eur. Phys. J. B **6**, 183 (1998).
[39] F. Varret, K. Boukheddaden, J. Jeftic, and O. Roubeau, J. Mol. Cryst. Liq. Cryst. **335**, 1273 (1999).
[40] A. R. Stokes and A. J. C. Wilson, Math. Proc. Cambridge Philos. Soc. **38**, 313 (1942).
[41] A. R. Stokes and A. J. C. Wilson, Proc. Phys. Soc., London **56**, 174 (1944).
[42] M. Hanawa, Y. Morimoto, J. Tateishi, K. Kato, M. Takata, and M. Sakata, J. Phys. Soc. Jpn. **72**, 987 (2003).
[43] E. Pytte, Phys. Rev. B **10**, 4637 (1974).
[44] G. Beni, J. Chem. Phys. **58**, 3200 (1973).
[45] C. Chong, Ph.D. thesis, Université de Versailles, 2010.
[46] C. Chong, A. Slimani, F. Varret, K. Boukheddaden, E. Collet, J.-C. Ameline, R. Bronisz, and A. Hauser, Chem. Phys. Lett. **504**, 29 (2011).
[47] I. Krivokapic, C. Enachescu, R. Bronisz, and A. Hauser, Chem. Phys. Lett. **455**, 192 (2008).